2009

Polyelectrolyte-linked, multi-layer film assemblies of aqueous nanoparticles and nanoshells

Anne Galyean
University of Richmond

Chemistry
Galyean

Polyelectrolyte-Linked, Multi-layer Film Assemblies of Aqueous Nano*particles* and Nano*shells*

Anne Galyean

Honors Thesis
The Department of Chemistry
University of Richmond
Richmond, VA

April 23, 2009

APPROVED BY:

ADVISOR

Michael Leopold
Department of Chemistry
University of Richmond

SECOND READER

Carol Parish
Department of Chemistry
University of Richmond

Table of Contents

Acknowledgements

First and foremost I would like to recognize my advisor and friend, Michael Leopold for academic and personal support during my undergraduate work at University of Richmond. The Leo research group also gratefully acknowledges the Howard Hughes Medical Institute and the University of Richmond Undergraduate Research Committee, College of Arts and Sciences for providing funding for this project. A special thanks to Carol Parish for being the second reader for this thesis. This work is due to the significant contributions to this work by Robert Day, Callie Dowdy as well as Justin Malinowski and Kevin W. Kittredge at Sienna College, and Carolyn Marks in the Department of Biology at Richmond for her assistance with TEM imaging. Special thanks is given to Drs. Tim Smith, Rene Kanters, Rob Miller and Will Case, as well as Russ Collins, Phil Joseph, Mandy Mallory, and John Wimbush - all of whom make undergraduate research possible at the University of Richmond.

Abstract

Multi-layer films of nanoparticles and nanoshells featuring various polymeric linkage molecules have been assembled and their optical properties characterized. The growth dynamics, including molecular weight effects, and stability of the various nanoparticle film constructions, using both single polymer as well as combinations of alternating charge polyelectrolytes as linking mechanisms, are presented. The polymeric linkers studied include poly-L-lysine, poly-L-arginine, poly(allylamine hydrochloride), and polyamidoamine dendrimers. Significantly air stable films were achieved with the use of multi-layered polymeric bridges between the nanoparticles and nanoshells. Optical sensitivity normally observed with these nanomaterials in solution was observed for their corresponding film geometries, with the nanoshell films exhibiting a markedly higher ability to report their local dielectric environment.

1. Introduction

Significant interest exists in the optical properties of metallic nanomaterials, such as nanoparticles (NPs), nanoshells (NSs), and nanotubes (NTs). Their observed optical sensitivity as a function of size, composition, dielectric environment, and geometric spacing makes these materials of particular interest for sensing technology development.[1-7] Thus, the integration of these nanomaterials into ordered arrays and layered assemblies remains an important topic of research in this field, especially thin films composed of nanoparticles (NPs) which have been explored as both sensory materials and used as surface modifiers for techniques such as SERS and surface plasmon resonance spectroscopy. [8] Gold NPs are usually synthesized with protective ligands in order to stabilize the metal core and prevent spontaneous aggregation to bulk metal. [9] The highly stable alkanethiol-based monolayer protected clusters (MPCs) with gold cores, synthesized by the Brust reaction, have been prominently investigated by Murray and various others. [10-11] Due to their superior stability and ease of functionalization, MPCs are a target material for developing two dimensional chemical sensors, a geometric arrangement more conducive to potential *in vitro* or *in vivo* sensing applications. To this end, MPCs have been assembled into films using various linking methods ranging from simple drop-cast materials [12-13] to complex, multilayered constructions. [14-18] Alkanethiolate-protected MPCs, although highly stable and easily functionalized, are limited in their sensing potential because of their lack of solubility in aqueous environments.

Recent work has focused on water soluble NPs surrounded by a variety of protective monolayers, the most common of which are citrate-stabilized NPs (CS-NPs) predominately studied in solution. [19] Natan and co-workers reported the attachment of CS-NP monolayers onto silanized glass and attempted to construct multilayered CS-NP films using various linking

mechanisms, such as dithiols, 2-mercaptoethanol, and 2-mercaptoethylamine ligands. However, CS-NPs are highly susceptible to aggregation, and cannot be reconstituted once extracted from an aqueous solution. [20] The instability of the CS-NPs in solution is visually evident over time and loss of NP integrity is readily observed in the spectroscopy of multi-layer films of the materials. Spectra of multi-layer CS-NP films tend to display properties of thin gold films (i.e., a severely red-shifted characteristic surface plasmon band (SPB)) rather than individual gold NPs simply networked within a scaffold. [19,21] In order to compensate for rapid aggregation of CS-NPs, Chen and co-workers developed a thioctic acid stabilization technique to construct negatively charged and highly solution stable NPs [20] (TAS-NPs), which can be used to assemble electrostatic-based and polymer linked multilayered films of substantial thickness with NP integrity maintained. [21]

A major area of research in the field of nanoparticle films is the use of polyelectrolye and polymer linking mechanisms, although most incorporate non-aqueous MPCs. Poly(allylamine hydrochloride) (PAH) and poly(4-styrene sulfonate) (PSS) have been explored individually and as combination polyelectrolyte linking mechanisms in several labs, including Murray's group [10] as well as Isaacs and coworkers, who also investigated the use of polyamidoamine dendrimers in these films [22]. Schmitt and Decher investigated sequential self assembly of aqueous NPs with various combinations of PAH, PSS, and poly(ethyleneimine) and determined that the film thickness of the polymeric multilayer films could be controlled using concentration, molecular weight, and ionic strength. [23] Later, they showed that flexible polyelectrolytes assembled into films do not form well-defined layers, but rather intermix to a significant degree with each subsequent polymer adlayer. [24] These findings were reiterated in molecular dynamic simulations performed by Dobrynin and coworkers [25] modeling polyelectrolyte films and

polyelectrolyte-linked NP assemblies which suggested structures of high porosity where polyelectrolytes effectively screen the NPs surface charges and allow them to fill gaps within the film. Work in our own lab continued this focus exploring poly-L-Lysine as a cationic polyelectrolyte linker in NP films. An early report by Bowden and co-workers used poly-L-Lysine (PL) as a bridging molecule between an adsorbed layer of the anionic protein cytochrome b5 and self-assembled monolayer of carboxylic acid terminated alkanethiols. [26] Burke and Barrett explored PL stability and strength in electrostatic films of PL and hyaluronic acid on charged silicon surfaces. [27] Simple monolayers of TAS-NP were found to be stable after extended exposure to both air and water whereas multilayered films showing similar stability in solution were observed to immediately aggregate upon significant contact with the ambient air. Thus, the use of PL as a linking bridge was highly successful for TAS-NP multilayered film growth, but limited in its sensing potential by air instability.

In this paper, we present a more comprehensive study of poly-electrolyte linked assemblies of TAS-NPs and, for the first time to our knowledge, extend the work to include films of nanoshells (NSs). The incorporation of NSs into film geometries is of significance considering the greater optical sensitivity observed for these materials in solution, a property our study shows translated to thin films as well. Film growth dynamics, including the effect of molecular weight, and overall film stability are studied for NP films with single polyelectrolyte as well as layered combinations of oppositely charged polyelectrolytes acting as linking bridges. The polymeric linking molecules used in this study are shown in Scheme 1 with the most successful/stable NP linking polymer combinations utilized to create films of nanoshells which exhibit greater sensitivity to changes in the local refractive index, a property of the material shown to persist in the film geometry.

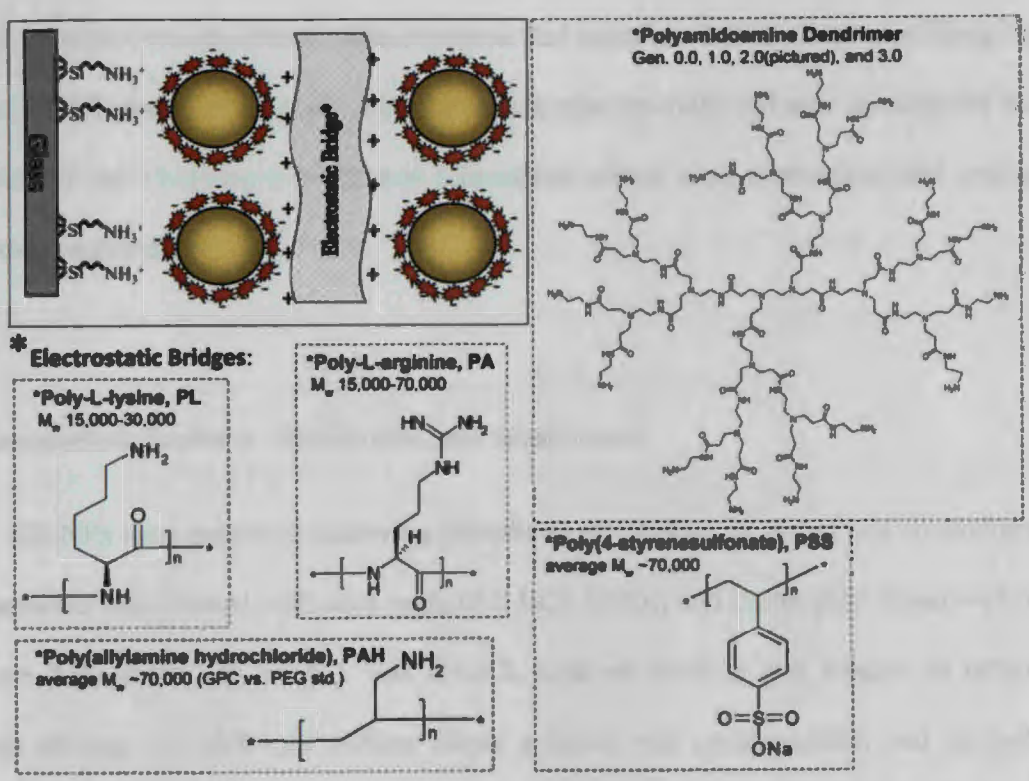

Scheme 1. Basic TAS-NP multilayer film with electrostatic bridge linked construction and various electrolyte and dendrimer linking materials used in film assembly.

2. Experimental

2.1. Chemicals

Poly-L-lysine (PL, MW 1,000-4,000; 15,000-30,000; >30,000), poly-L-arginine (PA, MW 15,000-70,000), poly(allylamine hydrochloride) (PAH, MW 15,000; 70,000), polyamidoamine dendrimers (PAMAM, Generation 0.0; 1.0; 2.0; 3.0), poly(4-styrene sulfonate) (PSS, MW 70,000; 75,000) were purchased from Sigma/Aldrich and used as received. All polymer linkers were dissolved in chilled sodium phosphate buffer (8.8mM, pH 8.5) to yield

0.5mM solution concentrations. Unsubstituted and substituted alkanethiol modifying ligands, used as 5 mM ethanolic solutions, were purchased commercially and used as received with the exception of the 15-crown-5 terminated alkanethiols which were synthesized and prepared as previously reported. [14, 28]

2.2. Nanoparticle Synthesis, Stabilization, and Modification

CS-NPs were produced following procedures established by Natan and co-workers. [19] All glassware was cleaned with aqua-regia (3:1 HCl, HNO_3) and thoroughly rinsed with 18MΩ ultrapure (UP) water. In brief, 1 mM $HAuCl_4$ aqueous solution was brought to reflux with constant stirring. A 38.8 mM sodium citrate solution was rapidly added, and the gold salt solution changed immediately from light yellow, to blue, to colorless, and finally to very dark red. The solution remained boiling at reflux for an additional 10 minutes before being allowed to cool to room temperature and vacuum filtered through a 0.8μM membrane filter (Gelman). Prior to further functionalization, the filtrate was stored in the dark at room temperature. CS-NP were characterized with UV-Vis spectroscopy (Agilent 8453 Photo Diode) and transmission electron microscopy (TEM). TEM imaging was performed at 80 kV with samples of drop-casted NP solution on 400 mesh copper grids coated with Formvar and carbon (Electron Microscopy Sciences).

The thioctic acid (TA) stabilization procedure developed by Chen and co-workers [20] was performed immediately following CS-NP synthesis to avoid aggregation. The pH of the CS-NP solutions was adjusted to pH 11 by adding 0.5 M NaOH dropwise in order to ensure charge

stabilization during TA functionalization. An equal molar quantity of TA to $HAuCl_4$ used in CS-NP synthesis was added to the CS-NP solution and stirred overnight in the dark. The exchange solution was then centrifuged at 15,900 g and 10 °C for 25 minutes (Sorvall RC-5B Refrigerated Superspeed). The supernatant was decanted, with the remaining dark red solid dissolved in equal parts UP water and stored in the dark until further use. TAS-NP solutions were characterized by TEM and UV-Vis spectroscopy as previously described (Figure1). [21]

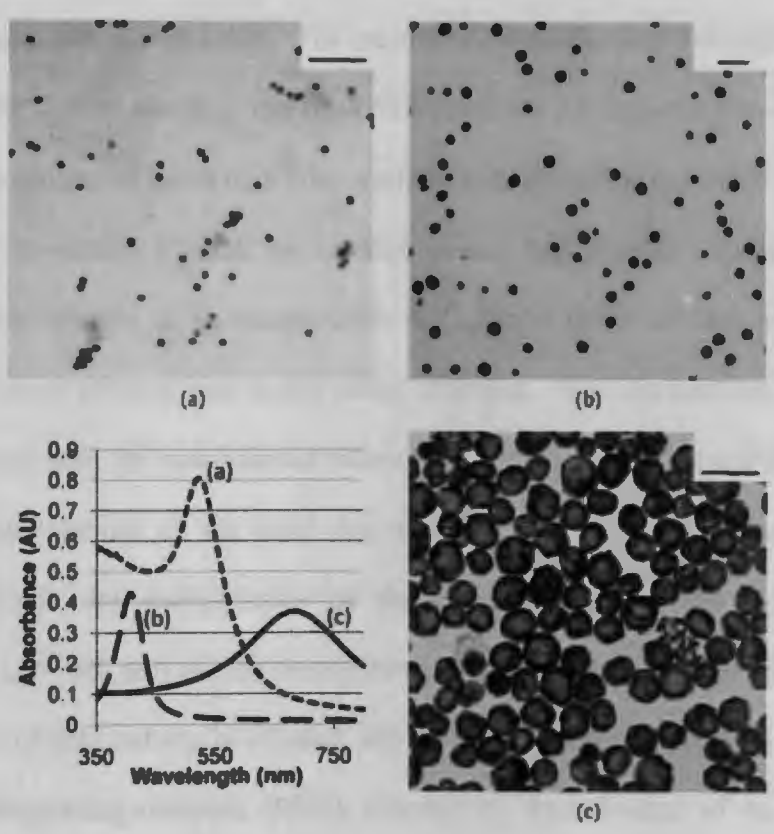

Figure 1. Typical TEM image and UV-Vis spectra of (a) TAS-NPs, TEM taken at 75,000x magnification; (b) Ag-NPs, TEM taken at 25,000x magnification; and (c) Au-NSs, TEM taken at 60,000x magnification. The bars in the lower right corners of the TEM images represent 100nm. [Note: Histogram analysis of TEM imaging is included in the Electronic Supporting Materials (ESM), Graphic 1]

2.3. Nanoshell Synthesis, Stabilization, and Modification

Hollow gold nanoshells (NSs), with an average diameter of approximately 30 nm were synthesized according to a procedure developed by Xia and Sun in which an aqueous solution of $HAuCl_4$ reacts with silver NPs, which serve as sacrificial templates [29] (see Figure 1). For a typical Ag NP synthesis [30], 0.400 g $AgNO_3$ (2.36 mmol) in 15 mL ethylene glycol was added to a solution of 10 g polyvinylpyrrolidone (PVP) (0.182 mmol) in 50 mL ethylene glycol upon the complete dissolution of both solids. The reaction mixture was then refluxed for ~12 hours in an oil bath at 120° C with stirring. The final PVP stabilized Ag nanoparticles were redissolved in 100 mL water and stored in the dark after washing with 200 mL acetone and centrifugation at 10,000 rpm for 20 minutes (Sorvall RC-5B Refrigerated Superspeed). To synthesize the Au nanoshells, a dilute solution of Ag nanoparticles was refluxed for 10 minutes, at which point a 1 mM $HAuCl_4$ aqueous solution was slowly added dropwise. With the addition of gold salt, the reaction progresses with the simultaneous reduction (deposition) of gold salt at the expense of the oxidation (dissolution) of the solid Ag templates and can be monitored by UV/Vis spectroscopy. Upon the disappearance of the surface plasmon band (SPB) of the Ag nanoparticles ($\lambda_{max} \sim 420$ nm) and the development of the SPB of the Au nanoshells ($\lambda_{max} \sim 680$ nm), the addition of gold salt was terminated, and the mixture was refluxed for a final 20 minutes (see electronic supporting materials (ESM), Graphic 2). Modification of Au nanoshells was accomplished by mixing a 5 mM mercaptoundecanoic acid (MUA) ethanol solution with the "as prepared" nanoshells in a 1:500 ratio for ~ 5 hours. The pH was adjusted to slightly basic conditions (~8) with aliquots of 0.5 M NaOH to ensure the retention of electrostatic repulsion of NSs from the terminal carboxylic acids during centrifugation at 10,000 rpm for 30 minutes. The

resulting pellet was then reconstituted in water for eventual incorporation into various film assemblies (*vida infra*).

2.4. Film Growth

Nanomaterial films were all grown using precut, Piranha-cleaned glass slides [*Warning! Pirahna solution (2:1 conc. H_2SO_4 to H_2O_2) reacts violently with organic materials, handle with extreme caution!]* Glass slides were silanized with 3-(aminopropyl)trimethyloxy silane (3-APTMS). [31] Films were grown using the "dip cycle" method, where growth materials are adsorbed onto the film by dipping the slides in alternating aqueous solutions. [14,18,28,32] The glass slides were dipped in either TAS-NP or PVP-NS solution for 1 hour followed by 30 minute dips in the respective linker solutions, and then again for 1h in NPs or NSs (dip cycle). The films were rinsed with UP water in between dip solutions, and stored in UP water. PL, PAH, and PAMAM dip solutions were refrigerated during both film growth and storage. Film growth was monitored by UV-Vis spectroscopy (Agilent 8453 diode array) every two completed dip cycles by placing the glass slide in an UP water-filled cuvette. Dip cycles were repeated for eight layers, or until the multilayered film was of the desired absorbance, around 0.1 AU measured at 400 nm (NP) or 600 nm (NS), wavelength positions removed from the surface plasmon band (SPB) to avoid recording any optical changes affecting the size, shape or position of the SPB as a change in film absorbance/thickness. [16,18,28] In general, the initial monolayer or submonolayer of NPs on the modified glass substrate is pinkish-red in appearance, matching that of the NP dipping solution, and displays a spectrum featuring a SPB at 520 nm. Upon assembly of multiple layers, however, the NP film assemblies take on a purple appearance and

display a red shift of approximately 20 nm (540 nm). This phenomenon is shown in the ESM, graphic 3. The NS film assemblies, on the other hand, remain blue, like the NS solution, throughout the assembly process. Discrepancies in these general trends are discussed within the text.

3. Results and Discussion

3.1. Nanoparticle films with single polymer linkages

TAS-NP multilayered films were grown using a variety of different polyelectrolyte or dendrimer linking bridges (shown in Scheme 1), including poly-L-lysine (PL), poly-L-arginine (PA), poly(allylamine hydrochloride) (PAH) and polyamidoamine dendrimers (PAMAM). All multilayered films were anchored with a TAS-NP monolayer on 3-APTMS silanized slides, taking advantage of the electrostatic interactions between the carboxylic acid groups on the peripheral thioctic acid layer and the cationic amine groups on the silanized glass. [19,21] Spectroscopic analysis of the TAS-NP monolayer shows a defined SPB with a λ_{max} at 520 nm, confirming that the monolayer is stable in solution with no sign of aggregation.

The previously observed instability of films of aqueous NPs prompted a study of the effects of the molecular weight of the polymer linking bridges on both growth and stability. At small interparticle distances, the surrounding protective layers are often compromised and the NPs spontaneously aggregate. Larger molecular weight polymeric linkers may be more effective at maintaining insulation between NPs within the film and preventing aggregation. [23] Multilayer NP films were grown with varying molecular weights of PL films linking bridges:

low (MW 1,000-4,000), medium (MW 15,000-30,000), and high (MW >30,000). Figure 2A shows UV-Vis spectra growth comparisons of low, medium and high molecular weights PL, which appear to grow (increase in absorbance) at relatively the same rate. Measurements taken at the same dip cycle are seen to be higher with increased molecular weight, suggesting that the heavier polymers result in slightly larger absorbance/thickness [23] than those grown with the lighter polymer linkers. For example, after eight dip cycles, high MW PL films show an absorbance around 1.1 AU at 400 nm, compared to only 0.85 AU for the low MW PL. Additionally, the SPB of films grown with high MW PL is noticeably narrower and displays a λ_{max} similar to that of a TAS-NP solution, especially compared to films grown with low MW PL which have broader and more red-shifted SPBs. This suggests that the higher MW polymer linkers are successfully limiting NP-NP interactions.

When a film being grown in low MW PL is abruptly grown using high MW PL, there is no visible change in the growth patterns. The average increase in absorbance between dip cycles remains relatively constant, and the SPB does not appear to red-shift or broaden. A similar result is observed for films grown with high MW PL that are then continued later with low MW PL; there is no significant change in film growth or properties. The indifference of the growth to the changes in the linker MW during assembly may indicate that once initial layers of NPs and polyelectrolytes are in place, the effect of MW is less substantial. The fact that the listed MW of the polyelectrolytes represents the average mass of the material is likely contributing to the lack of a distinctive MW effect.

PL films were shown to be very stable in solution, especially when compared to the previously used dithiol-linked NP films. [21] However, although the films are stable in solution

with no signs of aggregation for at least 50 days,[21] there is obvious and rapid aggregation of the NPs in the film within seconds after exposure to ambient air, resulting in a significant and irreversible red shift of the SPB (>600nm) accompanying very significant broadening of the SPB. Additionally, the film's appearance was abruptly and significantly changed upon exposure to air, taking on a thin metal film luster.

Films grown with PA (MW 15,000-70,000) showed unusual film growth with broadened SPBs (see ESM, graphic 4), and were not stable in solution or air. PA itself is not totally soluble in the sodium phosphate buffer solution used to make linker dips. UV-Vis spectra during film growth indicate that PA-linked films grow more slowly than films grown with other single bridge linkers, since there is less of an absorbance increase in between dip cycles compared to other film constructions. Due to the instability of the PA linked multilayer films, further investigations of these films were not explored. With similar structures, the notable difference between the PA-linked system versus the PL-linked system described above is not completely understood, but is likely related to the bulkier cationic end groups of PA (Scheme 1) being problematic as part of an electrostatic linking bridge.

PAH films grew relatively well compared to the PL and PA systems, exhibiting an absorbance of 1.2 AU after 8 dip cycles. This growth appeared to be in spite of the fact that PAH was sparingly soluble in the buffer solution with the resulting films being visibly and uncharacteristically cloudy, suggestive of an unidentified complexity within the assembly scheme. Figure 2B demonstrates the growth patterns of PAH (MW 15,000), which resulted in films that grew inconsistently and frequently caused the TAS-NPs to crash out of solution during the NP dip. PAH (MW 70,000) resulted in slightly more consistent growth patterns, but still

presented a red-shift during film growth and grew to only a slightly higher absorbance compared to the low MW PAH. The SPBs of PAH films are significantly broader than that of the PL films (Figure 2 comparison). Even though PAH films display some instability during the film growth process, they were relatively stable in solution. Unfortunately, the PAH films do aggregate within seconds upon contact with air.

Recent research performed by Isaacs and co-workers examined overall stability of multilayer NP assemblies using metal cation, ionic polymer and dendrimer linking constructions. [22] Their success prompted us to incorporate dendrimer molecules into NP film constructions, in order to further explore molecular weight effects. Various generations of PAMAM dendrimers were used to grow multilayered films, and showed very similar growth dynamics to molecular weight comparisons of PL films (Figure 2C). Generation 3.0 consistently grew to a higher absorbance compared to Generation 2.0, which was subsequently higher than 1.0 and 0.0, respectively. All PAMAM films grew at relatively the same rate, with minimal red-shifting of the SPB, but to a lower overall absorbance than both the PAH and PL films. Similar to the PL linked films, higher molecular weight linking molecules appear to result in films with slightly higher final absorbances. With all the films exhibiting similar growth rates, the observed subtle increases with MW appear to be related to differences in the initial anchoring layers of the film. Additionally, multi-layered PAMAM films appear pink throughout the growth sequence rather than the characteristic purple tint observed for the other single bridge linked multi-layer films. The lack of a color change normally attributed to more compact films may be the result of the bulkier dendrimer linking maintaining greater interparticle spacing. Alternatively, the NPs within the PAMAM-linked film may be experiencing a slightly different dielectric environment

compared to the polyelectolyte films previously discussed. [8] As with the other single polymer bridged films, PAMAM films aggregate upon air exposure.

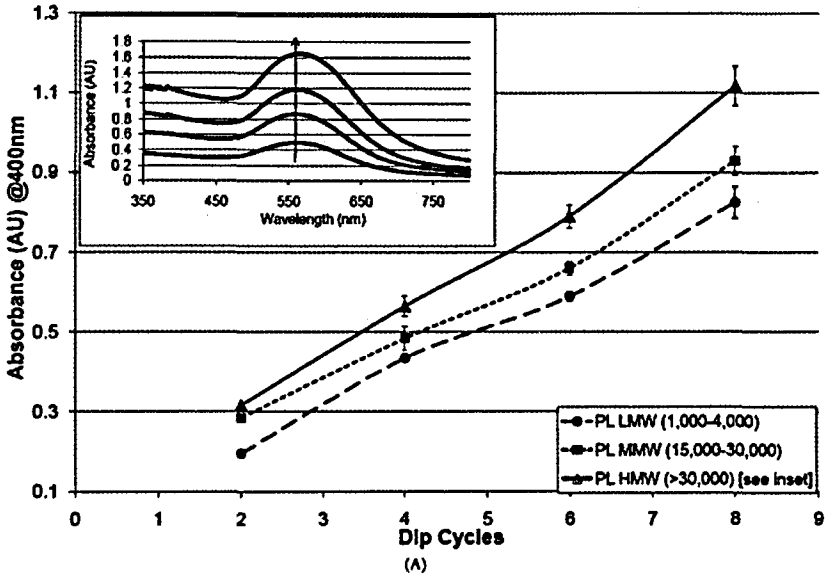

(A)

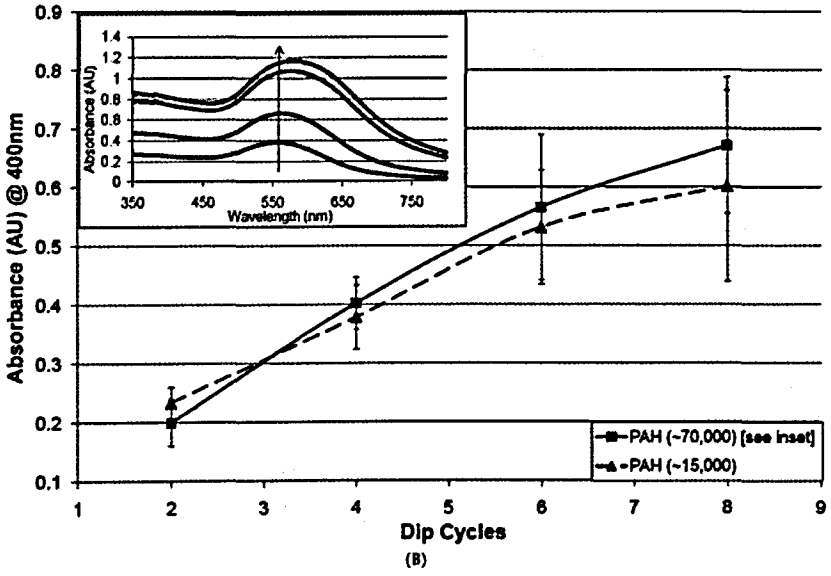

(B)

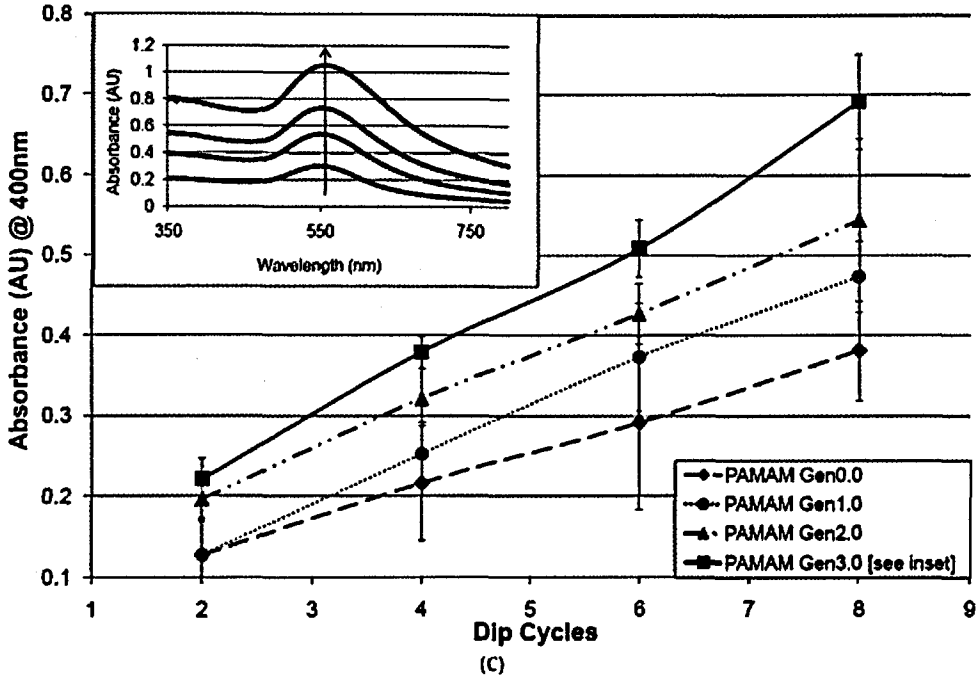

Figure 2. **(A)** Comparison of poly-L-lysine (PL) linked NP films, showing differences in growth dynamics between low (LMW), medium (MMW), and high (HMW) molecular weight PL (n =2); **(B)** Comparison of poly(allylamine) hydrochloride (PAH) linked NP films, showing differences in growth dynamics between high MW PAH (MW ~70,000) and low MW PAH (MW ~15,000) (n ≥3); **(C)** Comparison of poly(amidoamine) dendrimer (PAMAM) linked NP films, showing differences in growth dynamics between dendrimer generations 0.0, 1.0, 2.0 and 3.0 (n ≥4); **Insets (A-C):** UV-Vis spectra of film growth with HMW PL, PAH, and PAMAM (G3.0), monitored every 2 dip cycles. Note: The error bars refer to the standard deviation of an average based on measurements of a specific number of films (n). Some points have error bars that are smaller than the marker associated with that average.

Overall, PL and PAMAM films showed excellent stability while in solution and slightly increased growth with higher molecular weight. Similarly, PAH films remained stable in solution, but resulted in a broad SPB and growth that was not considerably influenced by molecular weight effects. PA films tended to aggregate during film assembly, and grew very

slowly. None of the multilayered films with single linker bridges showed any sign of air stability, as all aggregated immediately upon air exposure. We attributed this instability to the close proximity of the NP cores in these film constructions. Since NP films are known to swell in solution [17], the loss of solvent causes the film layers to shrink and the NP cores immediately aggregate upon drying out. Thus, other than a slight improvement in growth efficiency, it was concluded that polymer MW was largely inconsequential for air stability, an important characteristic if these films are to be considered for *in vitro* sensing applications requiring repeated exposure to solution and air.

3.2. Nanoparticle films with layered combinations of polymeric linkages

In an effort to achieve air-stable NP film assemblies, films featuring layered polyelectrolyte linking bridges were investigated with the thought that more layers of linking material between the NPs may increase the air-stability of the film. Linking mechanisms for multilayer film construction utilizing the electrostatic interactions between polyelectrolytes have been investigated by Schmitt and Decher, especially the use of alternating charged polymeric materials to provide multiple interactions between film layers. [23] PAH and poly(4-Styrene sulfonate) (PSS) was a combination frequently explored [10,22,33], however, it was not a particularly successful linking mechanism for TAS-NP multilayered films. PAH/PSS films showed severe aggregation during film growth, evidenced by a broad and red-shifted SPB, and further aggregation occurred upon air exposure. The successful growth of high MW PL as a single bridge linker inspired exploration of systems utilizing the PL linker in combination with PSS in an effort to assemble films with greater interparticle distances. Multilayered films of NPs

linked with alternating layers of PL and PSS were constructed using the same dip method as the single bridge linked films (Scheme 2). The films grew at a reasonable rate, although slightly less than that of the single PL films (see Figure 3A). The layered bridge films remained noticeably more of a pink color, not turning purple during growth as an indication of aggregation induced by smaller interparticle spacing, and had a significantly sharper SPB compared to single PL linked NP films. As seen in Figure 3B, the increasing number of polymer layers between the NPs (NP/PL/NP vs. NP/PL/PSS/PL/NP vs. NP/PL/PSS/PL/PSS/PL/NP) resulted in a corresponding blue shift of the SPB toward TAS-NPs in solution (i.e., not incorporated into a film assembly), indicating that the NPs within the film are experiencing greater interparticle distances and spacing that allows behavior more consistent with independent NPs. [34]

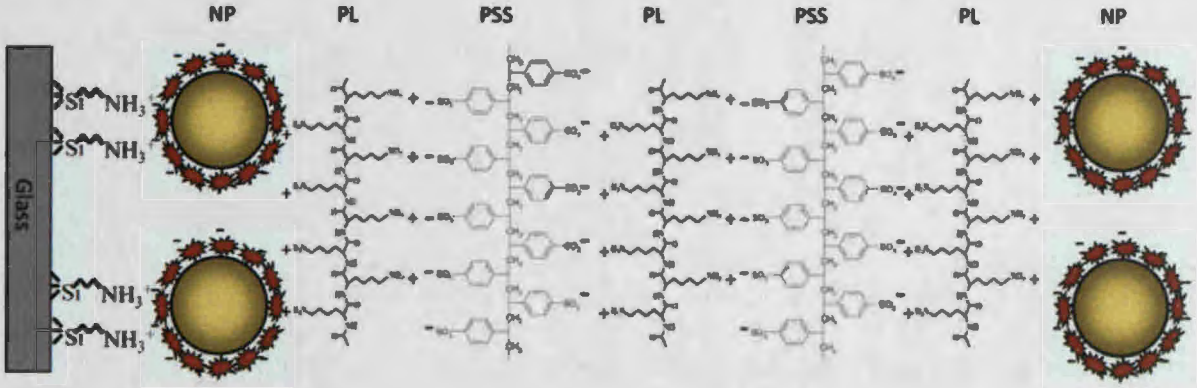

Scheme 2. Shows PL/PSS/PL/PSS/PL linked TAS-NP film construction. Film material not shown at scale.

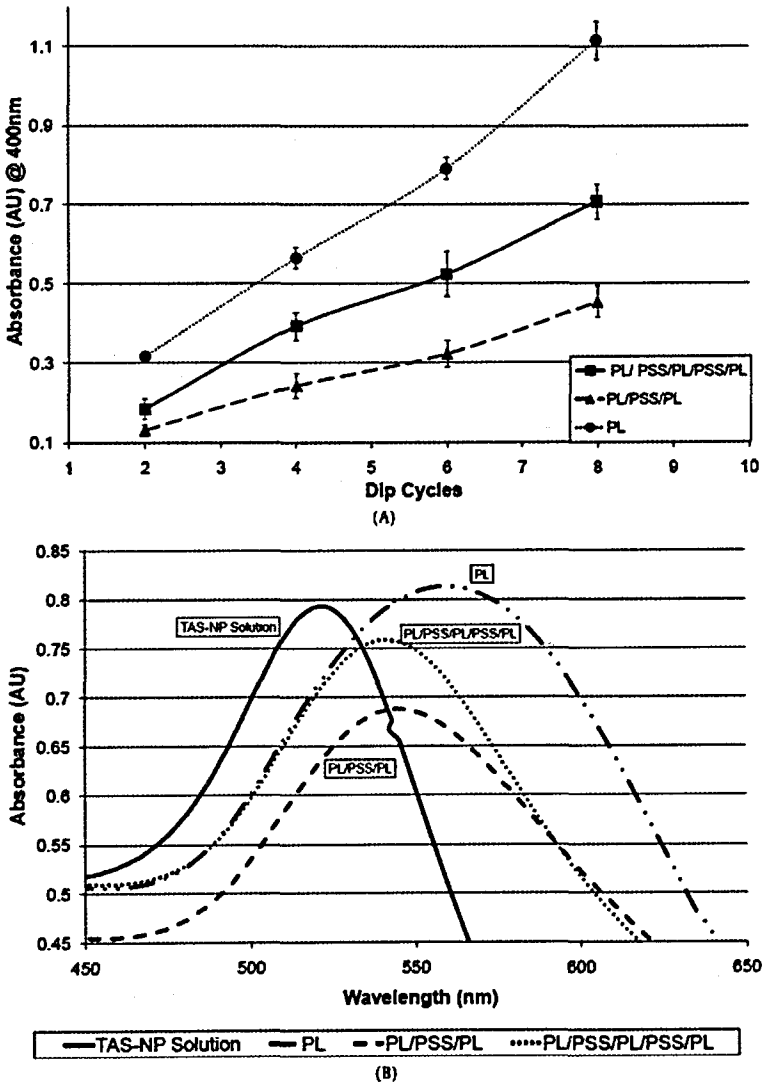

Figure 3. **(A)** Comparison of various poly-L-Lysine (PL) linked NP films, showing differences in growth dynamics between single bridge linked (n= 4), PL/PSS/PL linked (n=4), and PL/PSS/PL/PSS/PL linked constructions (n = 8); Note: The error bars refer to the standard deviation of an average based on measurements of a specific number of films (n). Some points have error bars that are smaller than the marker associated with that average. **(B)** UV-VIS spectra showing SPB of final dip PL, PL/PSS/PL and PL/PSS/PL/PSS/PL multilayer TAS-NP films compared to TAS-NP solution. Absorbance values in solution and film spectra are not indicative of stability but rather differences in concentration.

The air stability of these multi-polymeric linked films is tracked in Figure 4 where the spectroscopy of the films is compared before and after exposure to air. As previously discussed, the SPB of the PL-linked film undergoes a substantial, irreversible red shift and broadening as solvent leaves the film. In the films linked with PL/PSS/PL, the shift is smaller and with films featuring the PL/PSS/PL/PSS/PL linking bridge the SPB position and shape are preserved, exhibiting no red shift. These results suggest that the use of multiple linking layers within the film does indeed deliver the necessary architecture for an air-stable assembly – a significant finding if these films are targeted as a reusable and transportable commodity for certain sensing applications.

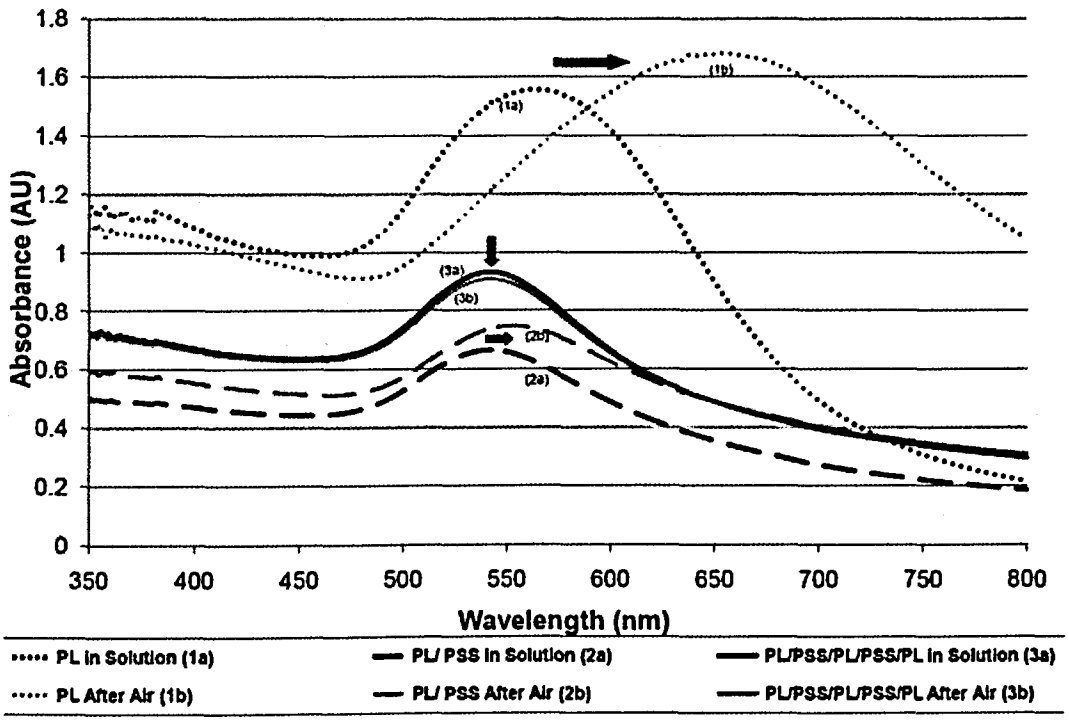

Figure 4. UV-Vis spectra showing the SPB of (1) PL linked TAS-NP films, (2) PL/PSS/PL linked films, and (3) PL/PSS/PL/PSS/PL linked films, both (a) in solution and (b) in solution after exposure to air.

3.3. Nanoshell films with layered combinations of polymeric linkages

Metallic nanoshells (NSs) have received significant interest because of their unique optical properties with most reports to date focusing on the characterization of their size, shape, and spectroscopic response of these materials in solution. [35] For example, hollow metallic NSs are of interest because they are known to exhibit greater optical sensitivity in solution compared to their solid core NP counterparts. [3] In terms of two-dimensional geometries, Halas and coworkers have explored NSs featuring a silica core surrounded by a thin metal coating as a possible plasmonic sensing element. [36] In this work, we extend the successful linking systems used for air-stable NP films to assemble stable *multi-layer films* of hollow gold NSs with the goal of capturing their unique optical sensitivity in a film geometry. NSs were synthesized from Ag NPs as previously described in the literature, [3] producing NS that are stabilized with polyvinylpyrrolidone (PVP). The PVP-NSs were then functionalized with carboxylic acid groups via a traditional exchange reaction involving 11-mercaptoundecanoic acid (MUA) as described in the experimental section. The negatively charged MUA-substituted PVP-NSs were treated in the same manner as TAS-NPs (*vida ante*). Figure 5A tracks the growth of NS versus NP film assemblies utilizing the multi-layer linkage system previously found to provide air stability (i.e., --/PL/PSS/PL/PSS/PL/--). While the growth is consistent and produces a stable film exhibiting a SPB (Figure 5A, inset), it should be noted that the solutions of NS were viable for only 4-5 dip cycles before the NSs would crash out of solution. The reasons for spontaneous aggregation are not readily apparent but may be caused by intermolecular hydrogen bonding induced between MUA-MUA interactions of neighboring NSs. Alternatively, some NP solutions aggregate upon contamination or leeching of the linkage materials into the solution from the film as the dip cycles progress. [17] The net result of our experiments, even with the

caveat of having to renew the NS solutions during the dipping cycles, are air-stable films of networked NSs (NS/PL/PSS/PL/PSS/PL/NS). The spectra of these NS films before and after exposure to air and compared to solutions of NS is shown in Figure 5B. It should also be noted that NS films with a fewer linking layers (i.e., NS/PL/PSS/PL/NS) were also found to have significant air stability (results not shown).

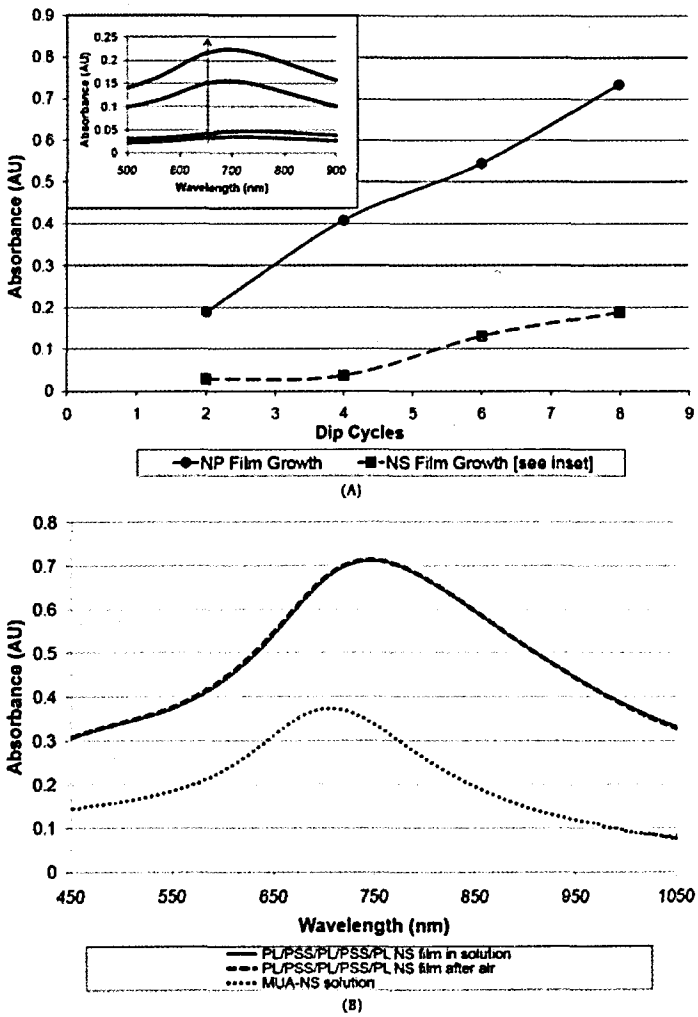

Figure 5. **(A)** Comparison of PL/PSS/PL/PSS/PL linked film constructions of NPs versus NSs. **Inset:** UV-Vis spectra of NS film growth monitored every 2 dip cycles; **(B)** UV-Vis spectra showing SPB of (a) NS film in solution, (b) NS film after exposure to air, and (c) a solution of NSs provided for comparison.

3.4. Optical properties: Nanoparticles versus Nanoshells

The size, shape, and position of the SPB in the spectra of metallic nanomaterials such as those investigated in this study are sensitive to changes at their surfaces and thus can act as tiny optical sensors that are sensitive to changes in their local environment, including molecular binding events. [8] To compare the optical sensitivity of both NPs and NSs toward binding events at their surfaces, the PVP-protected NSs as well as PVP-stabilized NPs made with a slightly modified procedure designed for the silver NP templates (using a 5:1 PVP to Au salt ratio) [30], were systematically modified in solution with different chainlengths of ω-substituted alkanethiol derivatives terminated in methyl (unsubstituted), hydroxyl, carboxyl, or ionophoric functional groups. In the latter case, 15-crown-5 terminated alkanethiols were included in the testing group since films of nanomaterials have been explored for metal sensing applications. [28] Substituted alkanethiols were targeted here because of their inherent ability to bind to gold surfaces and specifically alter the local dielectric environment at the NP/NS surface. Here, the absorbance maximum (λ_{max}) of each material's SPB was monitored before and after modification, and the shift ($\Delta \lambda_{max}$) was recorded as a function of chainlength (i.e., number of methylene units in the modifying ligand) in Figure 6. The observed trends indicate that an increase in the chainlength of the alkanethiol derivative is accompanied by a corresponding increase in the observed $\Delta \lambda_{max}$ for both the NPs and NSs in solution. Likewise, an obvious difference in sensitivity (i.e., slopes) exists between the NPs and NSs, with the NSs all exhibiting substantially higher $\Delta \lambda_{max}$ than the same ligands at NPs. Both of these trends reiterate results shown by Xia and coworkers with alkanethiol derivatives of NSs. [3] Of interest in our results is also the *insensitivity* of both systems to the different functional groups. With results falling

approximately at the same slope for each set of ω-substituted alkanethiol, the shifts in the SPB seem to be dependent only on the chainlength of the modifying ligands. Even when the NSs and NPs were augmented with a 15-crown-5 moieties that are most likely coordinated with sodium ions, the system remained unresponsive to the presence of the larger terminal group and the proximity of the cation. Collectively these results (Figure 6) reinforce the sensing mechanism of these materials is dictated by the localized dielectric environment of the NPs and NSs. The insensitivity of both materials to functional group changes at their periphery shows that refractive index changes from solution to the surrounding alkanethiol layer dominates the spectroscopic response even at more optically sensitive materials like NSs.

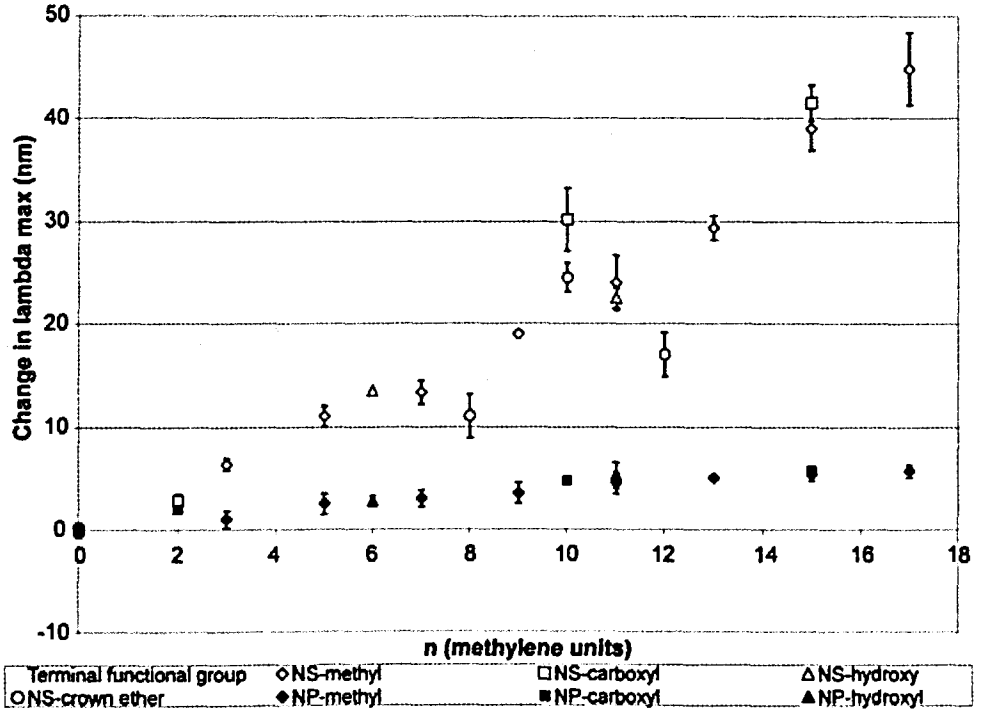

Figure 6. Changes in the λ_{max} of the SPB for solutions of PVP-protected NPs (solid symbols) and NSs (open symbols) as a function of the ω-substituted alkanethiol chainlength (i.e., methylene units, n) and terminal functional groups ($-CH_3$, -OH, -COOH, 15-crown-5). Note: The error bars refer to the standard deviation of an average based

on measurements of three different films. Some points have error bars that are smaller than the marker associated with that average.

For sensing applications, a two dimensional array of nanomaterials anchored to a substrate is often desired. In this work, we wanted to translate the aforementioned optical properties of the NS observed in solution to be functional for NS film assemblies. Assembled films of NSs connected with the combination polymeric linker system (NS/PL/PSS/PL/PSS/PL/NS) discussed above were constructed and subsequently exposed to solutions of butanethiol and tetradecanethiol (5 mM in ethanol). The SPB of the films was monitored before and after exposure to the modifying thiols with the results shown in Figure 7. The spectra clearly suggest that the materials have the same sensitivity trends observed for the solutions species. Both the NP and NS films show shifts upon exposure to thiols in solution, with longer alkanethiols resulting in more substantial spectral changes. However, as with these materials in solution (Figure 6), there is a stark contrast in the magnitude of the spectral shifts observed for films of NPs versus films of NSs, with the latter exhibiting substantially greater red shifts upon exposure to alkanethiols of significant length. Thus, the notable difference in sensitivity of NSs versus NPs is preserved, even when the materials are networked within film geometries with NSs remaining extremely sensitive to changes in refractive index.

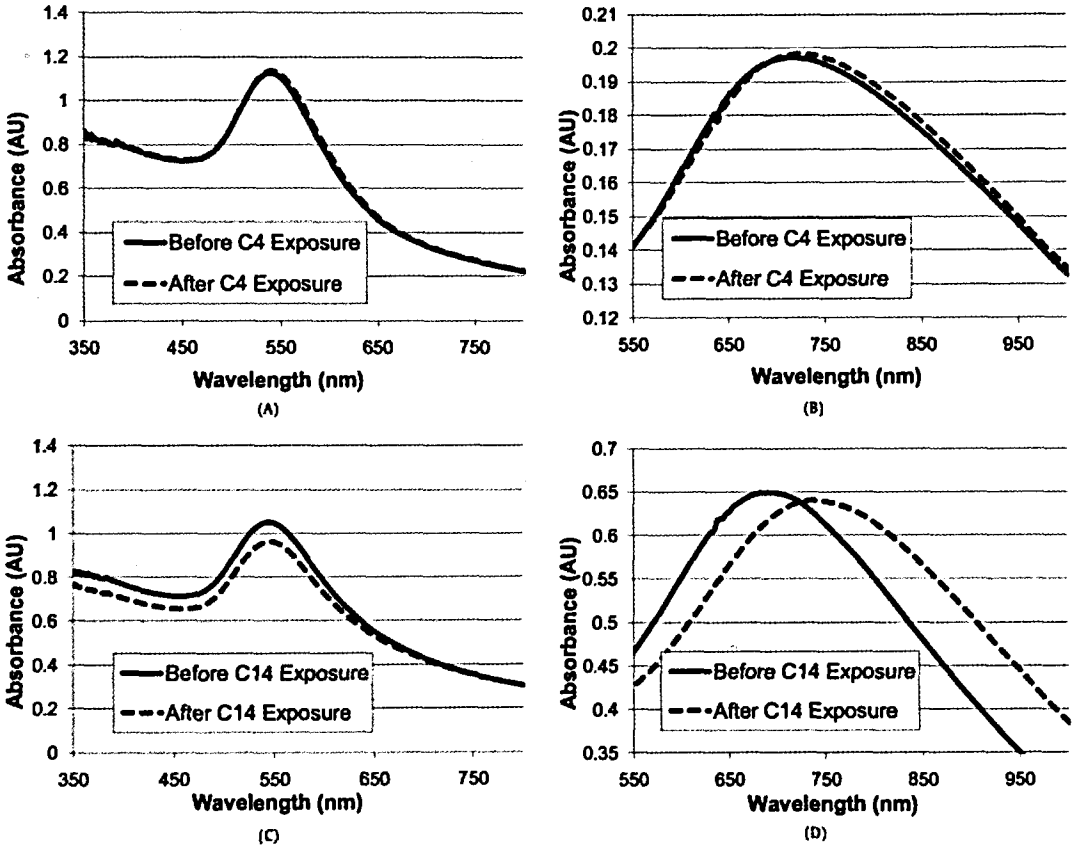

Figure 7. UV-vis spectra showing SPB of NP film **(A and C)** and NS films **(B and D)** before and after exposure to 5 mM butanethiol **(top)** and tetradecanethiol **(bottom)** ethanol solutions for 30 minutes followed by copious rinsing before being reimmersed in water for absorbance measurements.

4. Conclusion

Ordered assemblies of nanomaterials, while of potential interest to sensing technology, are more versatile materials for *in vitro* applications if they can be grown efficiently and are stable in both solution and air. In this study, we have successfully assembled and explored the growth dynamics of air-stable films of both NPs and NSs using a combinatorial strategy of polymer linking molecules that effectively maintains interparticle spacing and NP/NS integrity

(non-aggregation). The optical properties of these films revealed the materials within the film retained the ability to detect local changes to their dielectric environment and are sensitive to their specific spatial arrangements. As in solution, the NS films are observed to possess an inherently higher sensitivity in this regard, yielding more substantial wavelength shifts of the SPB upon exposure to alkanethiols in solution compared to the NP systems. The establishment of stable film structures of these materials should encourage further exploration of sensing applications, including ongoing studies in our own laboratory focused on using the films in the detection of a more diverse range of target molecules, perhaps capable of specific interfacial binding events (e.g., enzymes, ionophores).

References

[1] U. Kreibig, M. Vollemer, Optical Properties of Metal Clusters, Springer, Berlin, 1995.

[2] P. Mulvaney, Langmuir. 12 (1996) 788.

[3] Y. Sun, Y. Xia, Anal Chem. 74 (2002) 5297-5305.

[4] M.D. Malinsky, K.L. Kelly, G.C. Schatz, R.P. Van Duyne, J Am Chem Soc. 123 (2001) 1471.

[5] J.J. Storhoff, A.A. Lazarides, R.C. Mucic, C.A. Mirkin, R.L. Letsinger, G.C. Schatz, J Am Chem Soc. 122 (2000) 4640.

[6] H. Wang, D.W. Brandl, P. Nordlander, N.J. Halas, Acc Chem Res. 40 (2007) 53.

[7] M.E. Stewart, C.R. Anderton, L.B. Thompson, J. Maria, S.K. Gray, J.A. Rogers, R.G. Nuzzo, Chemical Reviews (Washington, DC, United States). 108 (2008) 494.

[8] A. Vaskevich, I. Rubinstein, Handbook of Biosensors and Biochips. 1 (2007) 447.

[9] M. Brust, J. Fink, D. Bethell, D.J. Schiffrin, C. Kiely, Journal of the Chemical Society, Chemical Communications. (1995) 1655.

[10] J.F. Hicks, Y. Seok-Shon, R.W. Murray, Langmuir. 18 (2002) 2288.

[11] D.L. Feldheim, C.A. Foss Jr. (Eds.), Metal Nanoparticles: Synthesis, Characterization, and Applications., 2002.

[12] Q. Cai, E.T. Zellers, Anal Chem. 74 (2002) 3533.

[13] S.D. Evans, S.R. Johnson, Y.L. Cheng, T. Shen, Journal of Materials Chemistry. 10 (2000) 183.

[14] L.E. Russell, R.R. Pompano, K.W. Kittredge, M.C. Leopold, J Mater Sci. 42 (2007) 7100.

[15] D. Sheibley, D.J. Tognarelli, R. Szymanik, M.C. Leopold, Journal of Materials Chemistry. 15 (2005) 491.

[16] D.J. Tognarelli, R.B. Miller, R.R. Pompano, A.F. Loftus, D.J. Sheibley, M.C. Leopold, Langmuir. 21 (2005) 11119-11127.

[17] F.P. Zamborini, M.C. Leopold, J.F. Hicks, P.J. Kulesza, M.A. Malik, R.W. Murray, J Am Chem Soc. 124 (2002) 8958.

[18] F.P. Zamborini, J.F. Hicks, R.W. Murray, J Am Chem Soc. 122 (2000) 4514.

[19] M.D. Musick, C.D. Keating, L.A. Lyon, S.L. Botsko, D.J. Pena, W.D. Holliway, T.M. McEvoy, J.N. Richardson, M.J. Natan, Chem Mater. 12 (2000) 2869.

[20] S. Lin, Y. Tsai, C. Chen, C. Lin, C. Chen, J Phys Chem B. 108 (2004) 2134-2139.

[21] L.E. Russell, A.A. Galyean, S.M. Notte, M.C. Leopold, Langmuir. 23 (2007) 7466.

[22] S.R. Isaacs, H. Choo, W.-. Ko, Y.-. Shon, Chem Mater. 18 (2006) 107.

[23] J. Schmitt, G. Decher, W.J. Dressick, S.L. Brandow, R.E. Geer, R. Shashidhar, J.M. Calvert, Advanced Materials (Weinheim, Germany). 9 (1997) 61.

[24] G. Decher, J.B. Schlenoff, (2003) 524.

[25] J. Jeon, V. Panchagnula, J. Pan, A.V. Dobrynin, Langmuir. 22 (2006) 4629.

[26] J.D.H. Glenn, E.F. Bowden, Chem Lett. 25 (1996) 399.

[27] S.E. Burke, C.J. Barrett, Biomacromolecules. 4 (2003) 1773.

[28] R.R. Pompano, P.G. Wortley, L.M. Moatz, D.J. Tognarelli, K.W. Kittredge, M.C. Leopold, Thin Solid Films. 510 (2006) 311.

[29] Y. Sun, B.T. Mayers, Y. Xia, Nano Lett. 2 (2002) 481-485.

[30] P. Silvert, R. Herrera-Urbina, K. Tekaia-Elhsissen, J Mater Chem. 7 (1997) 293-299.

[31] K.R. Brown, A.P. Fox, M.J. Natan, J Am Chem Soc. 118 (1996) 1154.

[32] A.C. Templeton, F.P. Zamborini, W.P. Wuelfing, R.W. Murray, Langmuir. 16 (2000) 6682.

[33] W. Zhao, J. Xu, C. Shi, H. Chen, Langmuir. 21 (2005) 9630.

[34] C. Lu, H. Moehwald, A. Fery, Journal of Physical Chemistry C. 111 (2007) 10082.

[35] Y. Sun, Y. Xia, Analyst (Cambridge, United Kingdom). 128 (2003) 686.

[36] L.R. Hirsch, J.B. Jackson, A. Lee, N.J. Halas, J.L. West, Anal Chem. 75 (2003) 2377.

Appendix 1: List of Figures

Figure 1. Typical TEM image and UV-Vis spectra of (a) TAS-NPs, TEM taken at 75,000x magnification; (b) Ag-NPs, TEM taken at 25,000x magnification; and (c) Au-NSs, TEM taken at 60,000x magnification. The bars in the lower right corners of the TEM images represent 100nm. [Note: Histogram analysis of TEM imaging is included in the Electronic Supporting Materials (ESM), Graphic 1]

Figure 2. **(A)** Comparison of poly-L-lysine (PL) linked NP films, showing differences in growth dynamics between low (LMW), medium (MMW), and high (HMW) molecular weight PL (n =2); **(B)** Comparison of poly(allylamine) hydrochloride (PAH) linked NP films, showing differences in growth dynamics between high MW PAH (MW ~70,000) and low MW PAH (MW ~15,000) ($n \geq 3$); **(C)** Comparison of poly(amidoamine) dendrimer (PAMAM) linked NP films, showing differences in growth dynamics between dendrimer generations 0.0, 1.0, 2.0 and 3.0 ($n \geq 4$); **Insets (A-C):** UV-Vis spectra of film growth with HMW PL, PAH, and PAMAM (G3.0), monitored every 2 dip cycles. Note: The error bars refer to the standard deviation of an average based on measurements of a specific number of films (n). Some points have error bars that are smaller than the marker associated with that average.

Figure 3. **(A)** Comparison of various poly-L-Lysine (PL) linked NP films, showing differences in growth dynamics between single bridge linked (n= 4), PL/PSS/PL linked (n=4), and PL/PSS/PL/PSS/PL linked constructions (n = 8); Note: The error bars refer to the standard deviation of an average based on measurements of a specific number of films (n). Some points have error bars that are smaller than the marker associated with that average. **(B)** UV-VIS spectra showing SPB of final dip PL, PL/PSS/PL and PL/PSS/PL/PSS/PL multilayer TAS-NP films compared to TAS-NP solution. Absorbance values in solution and film spectra are not indicative of stability but rather differences in concentration.

Figure 4. UV-Vis spectra showing the SPB of (1) PL linked TAS-NP films, (2) PL/PSS/PL linked films, and (3) PL/PSS/PL/PSS/PL linked films, both (a) in solution and (b) in solution after exposure to air.

Figure 5. **(A)** Comparison of PL/PSS/PL/PSS/PL linked film constructions of NPs versus NSs. **Inset:** UV-Vis spectra of NS film growth monitored every 2 dip cycles; **(B)** UV-Vis spectra

showing SPB of (a) NS film in solution, (b) NS film after exposure to air, and (c) a solution of NSs provided for comparison.

Figure 6. Changes in the λ_{max} of the SPB for solutions of PVP-protected NPs (solid symbols) and NSs (open symbols) as a function of the ω-substituted alkanethiol chainlength (i.e., methylene units, n) and terminal functional groups (-CH_3, -OH, -COOH, 15-crown-5). Note: The error bars refer to the standard deviation of an average based on measurements of three different films. Some points have error bars that are smaller than the marker associated with that average.

Figure 7. UV-vis spectra showing SPB of NP film **(A and C)** and NS films **(B and D)** before and after exposure to 5 mM butanethiol **(top)** and tetradecanethiol **(bottom)** ethanol solutions for 30 minutes followed by copious rinsing before being reimmersed in water for absorbance measurements.

Scheme 1. Basic TAS-NP multilayer film with electrostatic bridge linked construction and various electrolyte and dendrimer linking materials used in film assembly.

Scheme 2. Shows PL/PSS/PL/PSS/PL linked TAS-NP film construction. Film material not shown at scale.

Appendix 2: Supporting Information

Contents:

▶ TEM histogram analysis and representative images for thioctic-acid stabilized gold NPs, Ag nanoparticles, and gold NSs

▶ UV-Vis spectrum of gold NS formation from silver NP templates

▶ UV-Vis spectra illustrating SPB of gold NPs, in solution, as a monolayer/submonolayer immobilized on a substrate, and as multi-layers with polyelectrolyte linkages.

▶UV-Vis spectrum of PA multilayer film growth.

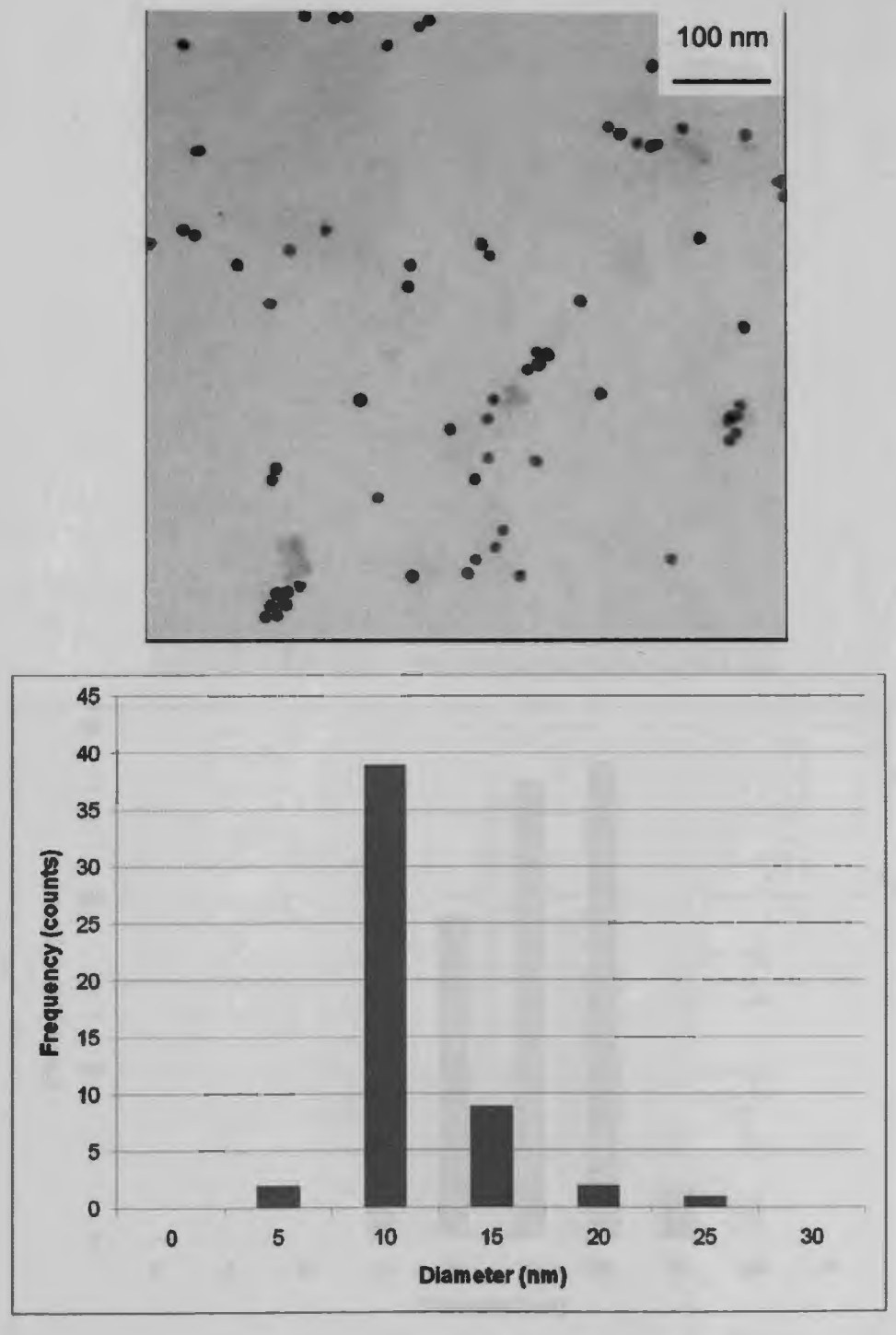

Figure SM-1 (a): Typical TEM image (*top*) of thioctic-acid stabilized gold nanoparticles. Core size histogram (*bottom*) from image analysis of TEM images indicates an average diameter of **9.63 ± 2.99 nm**.

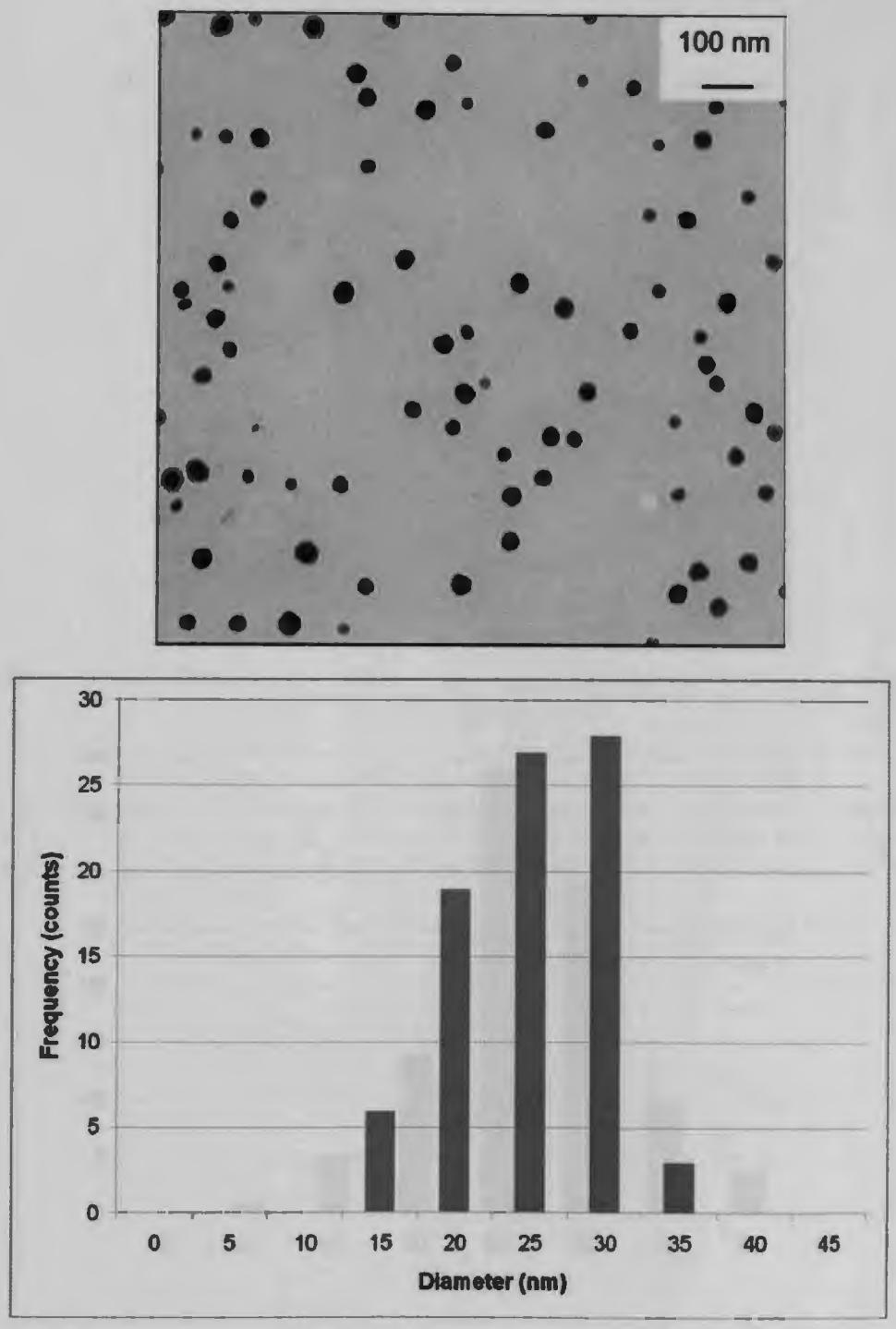

Figure SM-1 (b): Typical TEM image (*top*) of silver nanoparticles. Core size histogram (*bottom*) from image analysis of TEM image indicates an average diameter of **22.39 ± 4.82 nm**.

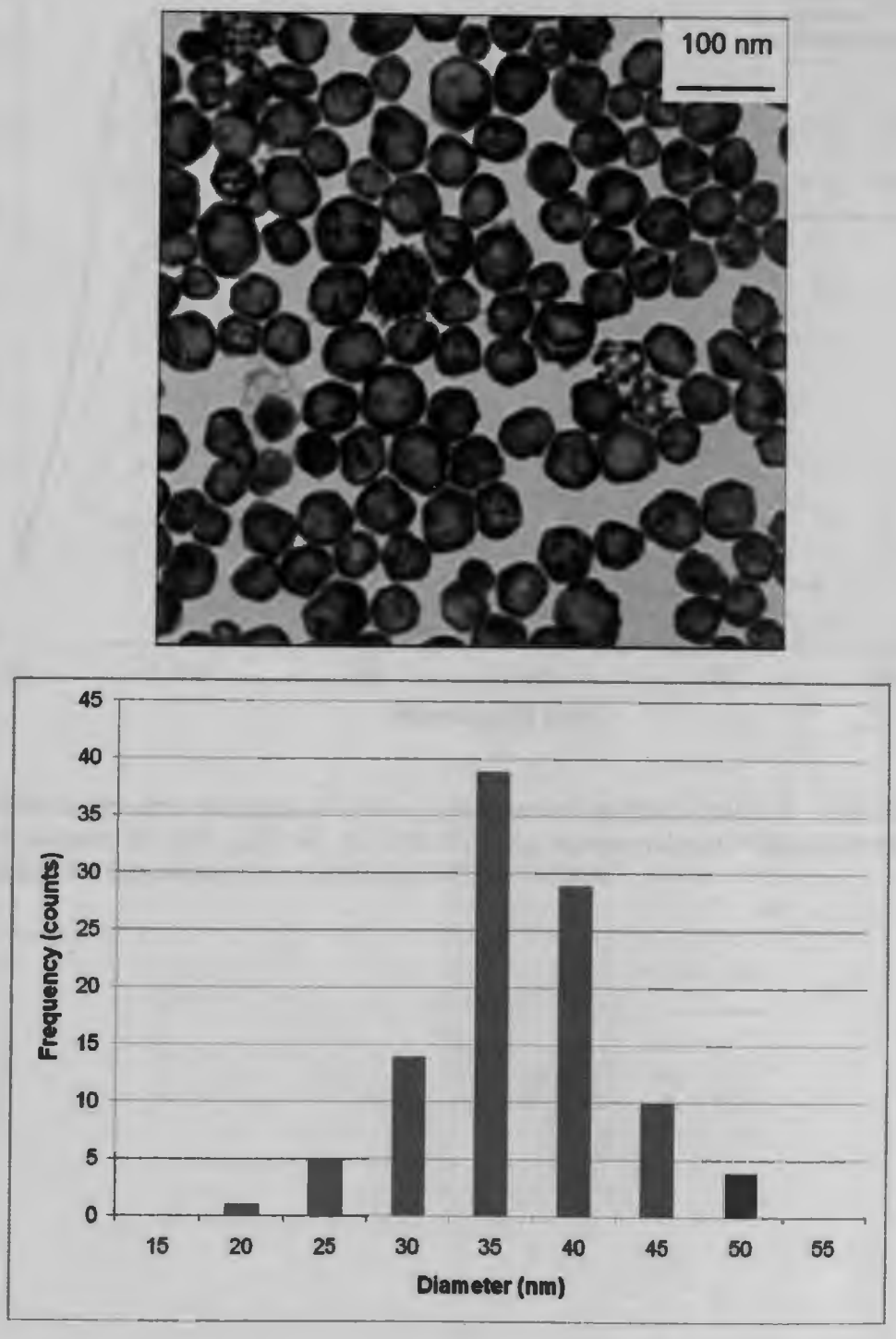

Figure SM-1 (c): Typical TEM image (*top*) of hollow gold nanoshells. Core size histogram (*bottom*) from image analysis of TEM images indicates an average diameter of **34.30 ± 6.30 nm**.

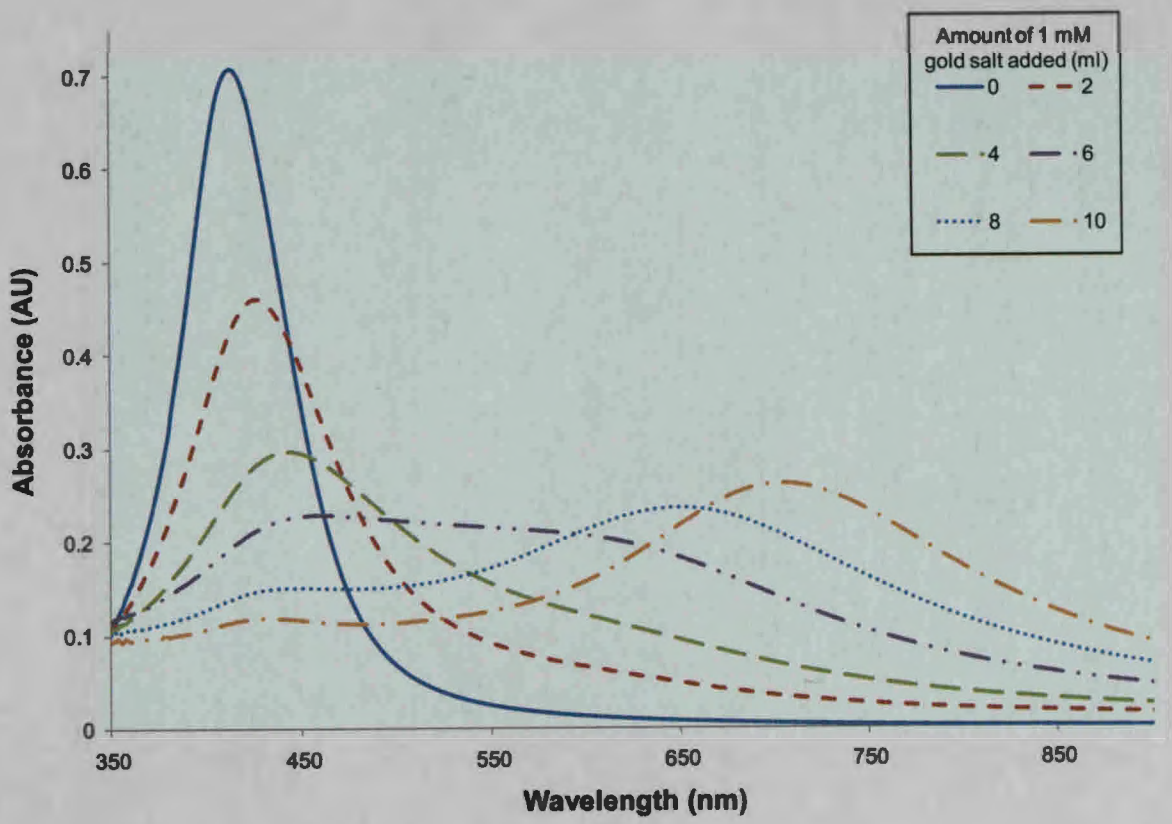

Graphic SM-2: Spectral evolution of hollow gold nanoshell synthesis reaction. With the addition of aliquots of 1 mM gold salt, the SPB of the Ag nanoparticles at ~420 nm decreases at the expense of the formation of the nanoshells' SPB at ~680nm.

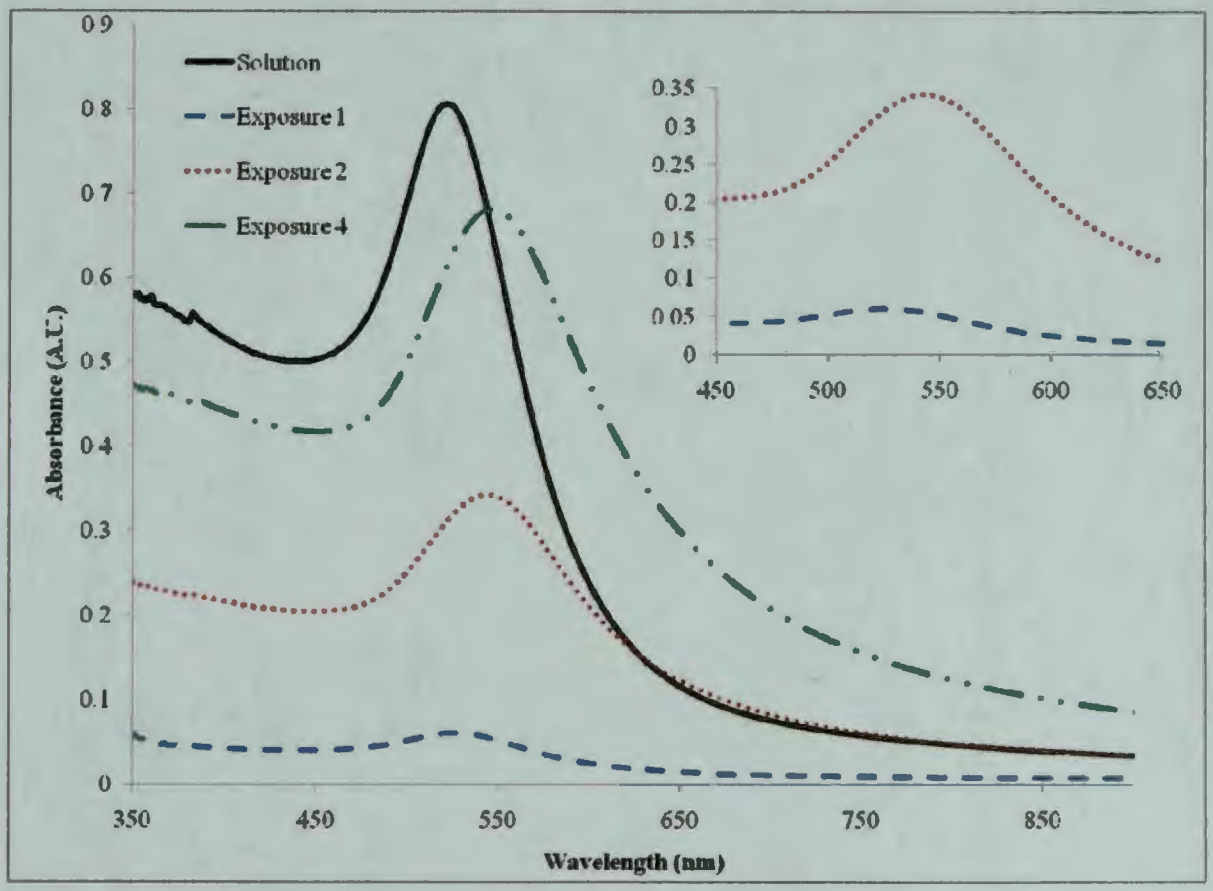

Graphic SM-3: UV-Vis spectra of TAS-NPs in solution (—) and immobilized on a modified glass substrate as a film consisting of an initial monolayer (- - -) of NPs formed from one exposure of the modified glass slide to the TAS-NP solution or as multi-layers of NPs linked with polyelectrolyte bridges (-PL/PSS/PL/PSS/PL-) after two (••••) and four (— •• —) growth cycles (i.e., alternate exposures to the TAS-NP solutions and polyelectrolyte linking layers).

Inset: Expanded spectra of the monolayer of TAS-NPs immobilized on glass and the multi-layer of TAS-NPs linked with -PL/PSS/PL/PSS/PL-. **Note:** It should be noted that the λ_{max} of the SPB is at ~520 nm for the particles in solution as well as for the first monolayer of NPs. However, as the multilayer is constructed, the SPB red shifts by ~20 nm with a λ_{max} at ~540 nm where it remains after further growth. All spectra of films were collected with the film immersed in solution (water) as described in the experimental details.

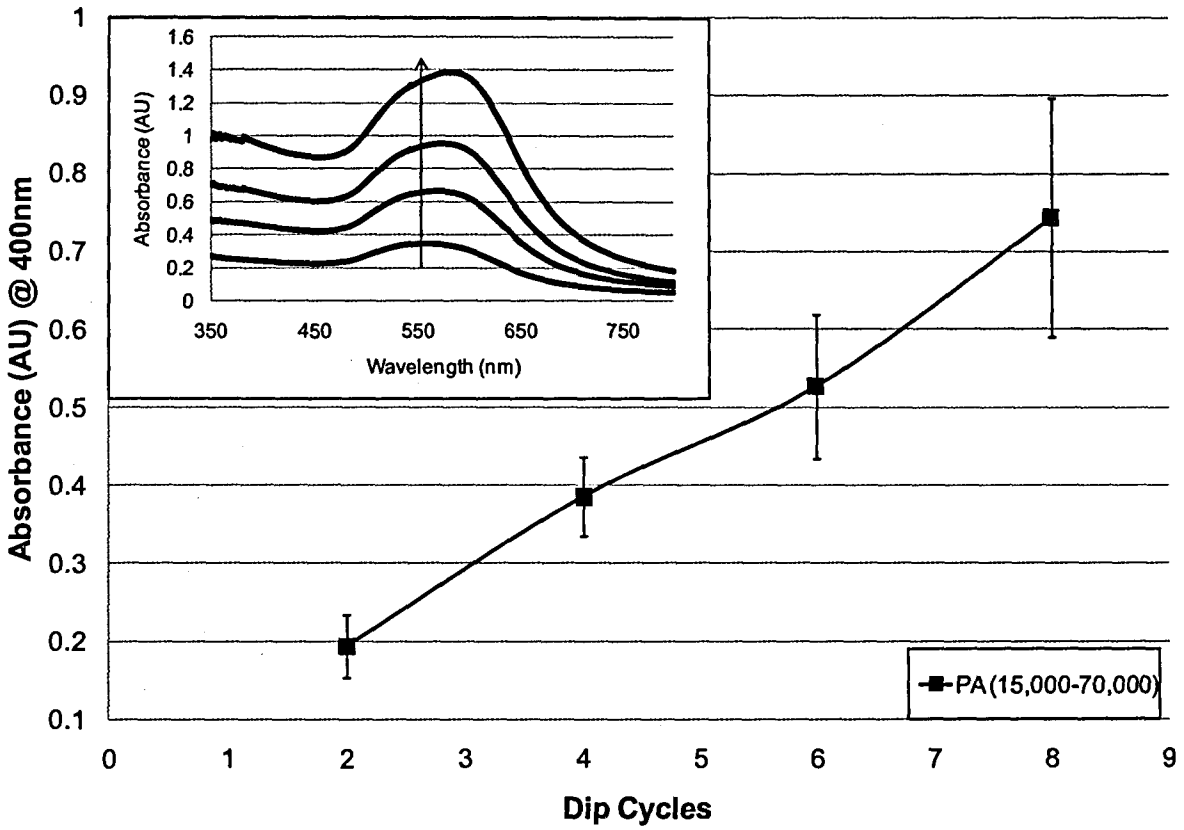

Graphic SM-4: UV-Vis spectra showing growth dynamics of poly-L-arginine (PA) linked NP films. **Inset**: UV-Vis spectra of film growth with PA, monitored every two dip cycles.